Cell-Free Massive MIMO: Zero Forcing and Conjugate Beamforming Receivers

Yao Zhang, Haotong Cao, Meng Zhou, and Longxiang Yang

Abstract: **In this paper, the uplink performance of cell-free massive multi-input multi-output (mMIMO) system with the zero-forcing (ZF) and conjugate beamforming (CB) receivers is investigated. A novel tight approximate rate expression for the ZF receiver is derived, which provides us with a tool for easily quantifying the impacts of the multi-antenna access point (AP), estimation error, pilot contamination, and power control scheme. Then, leveraging on the trackable ZF rate expression and the pre-studied CB rate expression, two power control algorithms are proposed. In particular, the first algorithm elaborates on maximizing the total rate, subjecting to the quality-of-service (QoS) constraint and each user power constraint. This algorithm utilizes the sequential convex approximation method to solve the non-convex issues. In addition, the second aims at maximizing the rate of one user, in which the remaining users can meet their QoS constraints. It can be characterized as a geometry programming. Simulation results are provided to show that the ZF receiver is superior to the CB receiver in terms of sum rate and our proposed algorithms work well in many respects.**

Index Terms: **Cell-free massive MIMO, conjugate beamforming, zero forcing, geometry programming, QoS constraint, sequential convex approximation.**

I. INTRODUCTION

AS a potential technology in the beyond fifth-generation (B5G) and sixth-generation (6G) networks, cell-free massive multi-input multi-output (mMIMO) system has been paid more and more attention by the academia and industry for its ability to perfectly integrate the merits of the network MIMO and distributed MIMO [1]-[5]. In such a system, the access points (APs) exist everywhere and each user can be coherently served by all APs. Different from the cellular mMIMO, there is no cell division in the cell-free system and the whole network can be regarded as one cell. In the whole serving area, each AP is equipped with limited computing power units and connected to a central processing unit (CPU) over a low-latency backhaul network for more advanced operations, such as calculating precoding coefficients and power control parameters. But

the high backhaul resource requirements in cell-free mMIMO system pose a severe challenge to the existing network structure [6], [7].

Cell-free mMIMO system has been extensively studied in the past few years. In particular, the authors in [1] investigated both the uplink and downlink rate performance of cell-free mMIMO system. It revealed that cell-free mMIMO system has considerably improved performance with respect to a small-cell system. In [2], the authors analyzed the radiated energy efficiency (EE) of the downlink mMIMO system for both cell-free and cellular modes. It demonstrated that the cell-free mode can double the radiated EE compared to the cellular structure. Besides, a sub-optimal total downlink EE maximization algorithm was proposed in [3]. The sequential convex approximation (SCA) method was then introduced to handle this non-convex issue. Its insightful findings highlighted the importance of the power optimization strategy. In [4], the authors presented some heuristic power control algorithms by converting the quasi-concave problems approximately into standard convex formulations, thereby, the computational complexity had sharply reduced. In addition, the authors in [5] combined the cell-free mMIMO system with the non-orthogonal multiple access (NOMA) technology. It suggested the NOMA can exploit the scarce spectrum bands more efficiently than the orthogonal multiple access.

However, all the above-cited contributions are mainly about the downlink performance, and there is relatively little research on the optimal power optimization for the uplink cell-free mMIMO system. For instance, the work of [8] derived the upper and lower-bound uplink rate expressions for uplink cell-free mMIMO system under both the perfect and imperfect channel state information (CSI) scenarios, but it did not characterize any power optimization schemes and the multi-antenna AP. In [9], the impact of the imperfect hardware transceivers on uplink cell-free mMIMO system was investigated. It also neglected any optimal power optimization. In addition, the authors in [10] proposed a max-min fairness power control algorithm for uplink cell-free mMIMO system, nevertheless, only the conjugate beamforming (CB) receiver was implemented. The CB receiver is computationally simple and can be implemented in a distributed manner. But the severe inter-user interference has still remained. More advanced receivers are urgently needed. Only very recently, in [11], the authors investigated the uplink performance of cell-free mMIMO system with the zero-forcing (ZF) and CB receivers and introduced three different resource control algorithms. It demonstrated that the ZF receiver can null out the inter-user interference, leading to a significant performance gain compared to the CB receiver. But pilot contamination is not covered in that paper.

Motivated by the above works, we consider an uplink cell-

free mMIMO system with the CB and ZF receivers. A tight approximate rate expression for the ZF receiver is derived. The specific contributions of this paper are summarized as follows:

1) We derive an uplink closed-form rate expression for the ZF receiver. This trackable finding provides us with a tool for easily quantifying the impacts of the multi-antenna AP, estimation error, pilot contamination, and power control schemes.

2) Two power control strategies based on the derived ZF rate expression and the pre-studied CB rate expression are proposed. In particular, the former aims at maximizing the uplink sum rate, subjecting to the quality-of-service (QoS) constraint and each user power constraint. It is non-convex, therefore, the SCA technique is adopted to handle this issue. Moreover, the second is one user's rate maximization problem. It is designed to maximize the rate of one user while ensuring that the remaining users can meet their QoS constraints.

3) A comprehensive performance comparison between the ZF and CB receivers is presented, with and without power optimization algorithms. It demonstrates that the ZF receiver is superior to the CB receiver in many respects. Nevertheless, since the ZF receiver needs more power to resist the inter-user interference, the total power consumption for the ZF receiver is higher than that of the CB receiver.

The rest of paper is structured as follows: System model and the time division duplex (TDD) mode are described in Section II. Section III investigates the uplink performance of the ZF receiver and presents the power optimization algorithms. The power optimization algorithms for the CB receiver are characterized in Section IV. Section V evaluates our analysis and Section VI concludes this paper.

Notation: In this paper, lower-case boldface letter denotes vector and matrix is represented by upper-case boldface letter. $\mathbf{A}^H$, $\mathbf{A}^T$ and $\mathbf{A}^*$ denote the conjugate transpose, transpose and conjugate of the matrix $\mathbf{A}$, respectively. $\|\mathbf{x}\|_2$ and $\|\mathbf{x}\|_1$ are the 2-norm and 1-norm of vector $\mathbf{x}$. $|\cdot|$ and $\mathbb{E}\{\cdot\}$ indicate absolute operator and expectation operator. $\mathbb{C}^{M \times 1}$ stands for a $M \times 1$ dimension complex space. Finally, $z \sim \mathcal{CN}\left(0, \sigma^2\right)$ means the complex Gaussian random variable, where the mean is zero and variance is σ^2.

II. SYSTEM MODEL

This paper considers an uplink cell-free mMIMO system where M APs coherently serve K users in a given area, $M > K$. We assume each AP is equipped with N antennas while each user only has one antenna. In this system, the APs utilize the same time-frequency block to provide services for all users. In addition, we further assume the whole system is operated in the TDD mode. In particular, each coherence interval consists of two phases: uplink pilot estimation and uplink data transmission. The former stage aims at estimating the uplink CSI. The so-obtained CSI will decode the uplink data in the next phase.

The $N \times 1$ dimension channel coefficient vector from the k-th user to the m-th AP can be modeled by

$$\mathbf{g}_{mk} = \beta_{mk}^{1/2}\mathbf{h}_{mk}, \tag{1}$$

where β_{mk} represents the large scale fading coefficient, which

reflects the effects of path loss and shadow fading. In addition, $\mathbf{h}_{mk} \in \mathbb{C}^{N \times 1}$ denotes the small scale fading vector, it is assumed $[\mathbf{h}_{mk}]_n \sim \mathcal{CN}\left(0, 1\right)$.

A. Uplink Channel Estimation

Prior to detecting the uplink data signal, the CPU needs to know the uplink CSI. Let τ be the length of the pilot sequence, which cannot be larger than the length of coherence interval, T. In fact, the number of pairwisely orthogonal pilots is limited by τ, and when $\tau < K$, the insufficient pilots will cause severe pilot contamination [1], which will hinder the system signal-to-interference-plus-noise ratio (SINR). In this paper, we consider the most aggressive case, where the CPU randomly allocates pilot to each user. Denote the pilot assigned to the k-th user is $\boldsymbol{\phi}_k \in \mathbb{C}^{\tau \times 1}$, where $\|\boldsymbol{\phi}_k\|^2 = 1$. After all users simultaneously transmitting their pilots to the APs, the m-th AP receives

$$\mathbf{Y}_{m,\mathrm{p}} = \sqrt{\tau \rho_{\mathrm{p}}} \sum_{k=1}^{K} \mathbf{g}_{mk}\boldsymbol{\phi}_k^H + \mathbf{W}_{m,\mathrm{p}}, \tag{2}$$

where ρ_{p} is the normalized transmit signal-to-noise ratio (SNR) associated with the pilot signal and $\mathbf{W}_{m,\mathrm{p}}$ denotes an $N \times \tau$ additive white Gaussian noise (AWGN) matrix whose elements are assumed to be independent and identically distributed (i.i.d.) random variables (RVs). Then, the m-th AP de-spreads the received pilots as

$$\tilde{\mathbf{Y}}_{mk,\mathrm{p}} = \mathbf{Y}_{m,\mathrm{p}}\boldsymbol{\phi}_k = \sqrt{\tau \rho_{\mathrm{p}}} \sum_{i=1}^{K} \mathbf{g}_{mi}\boldsymbol{\phi}_i^H\boldsymbol{\phi}_k + \mathbf{W}_{m,\mathrm{p}}\boldsymbol{\phi}_k. \tag{3}$$

Based on the minimum mean square error (MMSE) principle [12], the channel estimation of $\mathbf{g}_{mk}$ can be expressed as

$$\hat{\mathbf{g}}_{mk} = \frac{\mathbb{E}\left\{\mathbf{g}_{mk}\tilde{\mathbf{y}}_{mk,\mathrm{p}}^H\right\}}{\mathbb{E}\left\{\tilde{\mathbf{y}}_{mk,\mathrm{p}}\tilde{\mathbf{y}}_{mk,\mathrm{p}}^H\right\}}\tilde{\mathbf{y}}_{mk,\mathrm{p}} = c_{mk}\tilde{\mathbf{y}}_{mk,\mathrm{p}}, \tag{4}$$

where

$$c_{mk} = \frac{\sqrt{\tau \rho_{\mathrm{p}}}\beta_{mk}}{\tau \rho_{\mathrm{p}} \sum_{i=1}^{K} \beta_{mi}\left|\boldsymbol{\phi}_i^H\boldsymbol{\phi}_k\right|^2 + 1}. \tag{5}$$

The above expressions reveal that $\hat{\mathbf{g}}_{mk}$ contains the channels of other users who share the same pilot as the k-th user. In addition, the corresponding estimation error vector is given by

$$\tilde{\mathbf{g}}_{mk} = \mathbf{g}_{mk} - \hat{\mathbf{g}}_{mk}. \tag{6}$$

The statistics of $\hat{\mathbf{g}}_{mk}$ and $\tilde{\mathbf{g}}_{mk}$ are written as

$$\hat{\mathbf{g}}_{mk} \sim \mathcal{CN}\left(\mathbf{0}, \alpha_{mk}\mathbf{I}_N\right), \tilde{\mathbf{g}}_{mk} \sim \mathcal{CN}\left(\mathbf{0}, \left(\beta_{mk} - \alpha_{mk}\right)\mathbf{I}_N\right), \tag{7}$$

where

$$\alpha_{mk} = \frac{\tau \rho_{\mathrm{p}}\beta_{mk}^2}{\tau \rho_{\mathrm{p}} \sum_{i=1}^{K} \beta_{mi}\left|\boldsymbol{\phi}_i^H\boldsymbol{\phi}_k\right|^2 + 1}. \tag{8}$$

B. Uplink Data Transmission

In this phase, all users simultaneously transmit their data signals to the APs. Denote the data signal transmitted from the k-th user by s_k, where $\mathbb{E}\left\{|s_k|^2\right\} = 1$. Then the received signal at the m-th AP can be modeled as

$$\mathbf{y}_{m,\mathrm{u}} = \sqrt{\rho_{\mathrm{u}}} \sum_{k=1}^{K} \mathbf{g}_{mk} \sqrt{\eta_k} s_k + \mathbf{w}_{m,\mathrm{u}}, \qquad (9)$$

where ρ_{u} represents the normalized SNR related to the data signal, $0 \le \eta_k \le 1, \forall k$, refers to the power control coefficient and $\mathbf{w}_{m,\mathrm{u}}$ stands for an AWGN vector at the m-th AP. For signal detection, all APs need to deliver the received data signals to the CPU through the backhaul link. The aggregated received signals at the CPU can be written as

$$\mathbf{y}_{\mathrm{u}} = \sqrt{\rho_{\mathrm{u}}} \mathbf{G} \mathbf{P}^{1/2} \mathbf{s} + \mathbf{w}_{\mathrm{u}}$$
$$= \sqrt{\rho_{\mathrm{u}}} \sum_{k=1}^{K} \mathbf{g}_k \sqrt{\eta_k} s_k + \mathbf{w}_{\mathrm{u}}, \qquad (10)$$

where $\mathbf{G} = [\mathbf{g}_1, ..., \mathbf{g}_K] \in \mathbb{C}^{MN \times K}$, $\mathbf{g}_k = \left[\mathbf{g}_{1k}^T, ..., \mathbf{g}_{Mk}^T\right]^T \in \mathbb{C}^{MN \times 1}$ and $\mathbf{w}_{\mathrm{u}} = \left[\mathbf{w}_{1,\mathrm{u}}^T, ..., \mathbf{w}_{M,\mathrm{u}}^T\right]^T$. Besides, $\mathbf{P}$ models a power control diagonal matrix with the k-th element given by $[\mathbf{P}]_{kk} = \eta_k$. To detect the data signal of the k-th user, the CPU implements the lineal detector $\mathbf{A} \in \mathbb{C}^{MN \times K}$ to separate the received signal into streams, as

$$r_k = \sqrt{\rho_{\mathrm{u}}} \mathbf{a}_k^H \mathbf{G} \mathbf{P}^{1/2} \mathbf{s} + \mathbf{a}_k^H \mathbf{w}_{\mathrm{u}}$$
$$= \sqrt{\rho_{\mathrm{u}}} \sum_{i=1}^{K} \sqrt{\eta_i} \mathbf{a}_k^H \mathbf{g}_i s_i + \mathbf{a}_k^H \mathbf{w}_{\mathrm{u}}, \qquad (11)$$

where $\mathbf{a}_k$ is the k-th column of $\mathbf{A}$. Then, s_k will be detected from r_k.

III. ZF RECEIVER

In this section, it elaborates on investigating the uplink performance of cell-free mMIMO system with the ZF receiver. Firstly, a tight approximate uplink rate expression is derived. This closed-form result provides insights for the effects of multi-antenna AP, channel estimation error, pilot contamination, and power optimization strategies. In addition, two power optimization algorithms with the ZF receiver are proposed.

A. Achievable Rate for ZF Receiver

When the ZF receiver is implemented at the CPU, it has $\mathbf{A} = \hat{\mathbf{G}}\left(\hat{\mathbf{G}}^H \hat{\mathbf{G}}\right)^{-1}$, where $\hat{\mathbf{G}} = [\hat{\mathbf{g}}_1, ..., \hat{\mathbf{g}}_K]$ and $\hat{\mathbf{g}}_k = \left[\hat{\mathbf{g}}_{1k}^T, ..., \hat{\mathbf{g}}_{Mk}^T\right]^T$. The motivation behind the ZF receiver is the inter-user interference can be eliminated at the CPU, *i.e.*, $\mathbf{a}_k^H \hat{\mathbf{g}}_i = \delta_{ki}$, thereby significantly increasing the system performance. With the help of the ZF receiver, (11) can be recast as

$$r_k^{\mathrm{ZF}} = \sqrt{\rho_{\mathrm{u}} \eta_k} s_k + \sqrt{\rho_{\mathrm{u}}} \sum_{i=1}^{K} \sqrt{\eta_i} \mathbf{a}_k^H \tilde{\mathbf{g}}_i s_i + \mathbf{a}_k^H \mathbf{w}_{\mathrm{u}}, \qquad (12)$$

where the second term in (12) represents the estimation error term. Since the channel estimation and the estimation error is uncorrelated under the MMSE principle, the mean-square of the estimation error is given by

$$\mathbb{E}\left\{\left|\sqrt{\rho_{\mathrm{u}}} \sum_{i=1}^{K} \sqrt{\eta_i} \mathbf{a}_k^H \tilde{\mathbf{g}}_i s_i\right|^2\right\}$$
$$= \rho_{\mathrm{u}} \sum_{i=1}^{K} \eta_i \mathbb{E}\left\{\left|\mathbf{a}_k^H \tilde{\mathbf{g}}_i\right|^2\right\}$$
$$= \rho_{\mathrm{u}} \sum_{m=1}^{M} \sum_{n=1}^{N} |[\mathbf{a}_{mk}]_n|^2 \sum_{i=1}^{K} \eta_i (\beta_{mi} - \alpha_{mi}), \qquad (13)$$

where $[\mathbf{a}_{mk}]_n$ is the n-th entry of $\mathbf{a}_{mk}$. By virtue of [13], the exact ergodic uplink rate of the k-th user for the ZF receiver can be obtained as

$$R_k^{\mathrm{ZF}} = \mathbb{E}\left\{\log_2\left(1 + \mathrm{SINR}_k^{\mathrm{ZF}}\right)\right\}, \qquad (14)$$

where

$$\mathrm{SINR}_k^{\mathrm{ZF}} = \frac{\rho_{\mathrm{u}} \eta_k}{\rho_{\mathrm{u}} \sum\limits_{m=1}^{M} \sum\limits_{n=1}^{N} |[\mathbf{a}_{mk}]_n|^2 \sum\limits_{i=1}^{K} \eta_i (\beta_{mi} - \alpha_{mi}) + \|\mathbf{a}_k\|^2}, \qquad (15)$$

and where the outer expectation in (14) is with respect to $\mathbf{a}_k$. To calculate the uplink rate in (14), the CPU needs to know all realizations of $\mathbf{a}_k$, which will take a long time to average. Since the randomness of $\mathbf{a}_k$ is mainly dominated by $\mathbf{h}_{mk}$, it is necessary to find an approximation of (14) which is independent of $\mathbf{h}_{mk}$. Under this background, we derive a tight uplink rate expression for the k-th user in the following analysis, which is the function of β_{mk} only.

Theorem 1: With ZF receiver, a tight approximate uplink rate expression of the k-th user for any M, K, and N is formulated as

$$R_k^{\mathrm{ZF}} = \log_2\left(1 + \frac{\rho_{\mathrm{u}} \Omega(k) \eta_k}{\rho_{\mathrm{u}} \sum\limits_{i=1}^{K} \eta_i c_i + 1}\right), \qquad (16)$$

where

$$c_i = \arg\max_{m}(\beta_{mi} - \alpha_{mi}), \qquad (17)$$

$$\Omega(k) = \frac{\sum\limits_{m \in \mathcal{M}_k} \alpha_{mk}^2}{\sum\limits_{m \in \mathcal{M}_k} \alpha_{mk}}\left(\frac{N\left(\sum\limits_{m \in \mathcal{M}_k} \alpha_{mk}\right)^2}{\sum\limits_{m \in \mathcal{M}_k} \alpha_{mk}^2} - 1\right), \qquad (18)$$

$$\mathcal{M}_k = \{\forall m \ne m_{j*} | j \ne k\}, \qquad (19)$$

and

$$m_{j*} = \arg\max_m \beta_{mj}. \tag{20}$$

Proof: See Appendix A. □

Remark 1: Our rate approximation in (16) is very close to the case when all users enjoy the genie-aided CSI, *i.e.*, the channel $\mathbf{g}_{mk}$ is perfectly known. To highlight this point, we compare the performance difference between formulas (14) and (16) in Section V. In addition, since (16) is the function of β_{mk} only and β_{mk} varies slowly and remains unchanged during about 40 coherent intervals, our rate approximation is more tractable in the real-life scenario.

Remark 2: In (16), c_i denotes the biggest channel estimation error related to the i-th user. If the whole system suffers from less pilot contamination, the value of c_i will decrease, thereby increasing the achievable uplink rate of the i-th user. In other words, the performance of the ZF receiver is closely dependent on the accuracy of the channel estimation. The detailed simulation analysis for this insight will be presented in Section V.

B. Total Rate Maximization for ZF Receiver

In this subsection, it elaborates on finding the power control coefficients which maximize the total uplink rate for the ZF receiver, subjecting to the per-user power constraint and the QoS constraint. Mathematically, the total rate maximization problem for the ZF receiver is formulated as

$$P_1^{\text{ZF}} : \max_{\{\eta_k\}} \sum_{k=1}^{K} \log_2 \left(1 + \frac{\rho_\text{u} \Omega(k)\eta_k}{\rho_\text{u} \sum_{i=1}^{K} \eta_i c_i + 1} \right) \tag{21a}$$

$$s.t. \quad R_k^{\text{ZF}} \geq \bar{R}_k, \ \forall k \tag{21b}$$

$$0 \leq \eta_k \leq 1, \ \forall k, \tag{21c}$$

where constraint (21b) refers to the QoS constraint and $\bar{R}_k$ is the k-th user's QoS threshold. It remarks that P_1^{ZF} is complicated and neither concave nor convex with respect to η_k. In the previous work, [14] demonstrated that the power control problem like P_1^{ZF} is NP-hard and only can be determined in polynomial-time with non-deterministic computation. Besides, in [3], the authors indicated that the global optimal solution of P_1^{ZF} can be derived by using the branch-and-reduce-and-bound (BRB) method. Unfortunately, the cost of the BRB method is too high. Therefore, the low complexity SCA method given in [15], [16] enables us to handle this non-convex problem and find a high-performance solution. By defining $\varsigma_k = \eta_k^{1/2}$, P_1^{ZF} is equivalent to

$$P_2^{\text{ZF}} : \max_{\{\varsigma_k, t_k\}} \sum_{k=1}^{K} t_k \tag{22a}$$

$$s.t. \quad R_k^{\text{ZF}} \geq t_k, \ \forall k \tag{22b}$$

$$R_k^{\text{ZF}} \geq \bar{R}_k, \ \forall k \tag{22c}$$

$$0 \leq \varsigma_k \leq 1, \ \forall k, \tag{22d}$$

where

$$R_k^{\text{ZF}} = \log_2 \left(1 + \frac{\rho_\text{u} \Omega(k)\varsigma_k^2}{\rho_\text{u} \sum_{i=1}^{K} \varsigma_i^2 c_i + 1} \right). \tag{23}$$

To tackle (22b), we recall the following convex inequality [17]:

$$\ln\left(1 + \frac{x^2}{t}\right) \geq \ln\left(1 + \frac{\bar{x}^2}{\bar{t}}\right) + \frac{\bar{x}^2/\bar{t}}{1 + \bar{x}^2/\bar{t}}\left(2 - \frac{\bar{x}}{2x - \bar{x}} - \frac{t}{\bar{t}}\right)$$

$$\text{for} \ \forall x > 0, \ \bar{x} > 0, \ t > 0, \ \bar{t} > 0, \ 2x > \bar{x}. \tag{24}$$

With the help of (24), we have

$$\ln\left(1 + \frac{\rho_\text{u}\Omega(k)\varsigma_k^2}{H(\{\varsigma_k\})}\right) \geq \mathcal{L}\left(\{\varsigma_k\}, \left\{\varsigma_k^{(n)}\right\}\right)$$

$$= \ln\left(1 + \frac{\rho_\text{u}\Omega(k)\left(\varsigma_k^{(n)}\right)^2}{H\left(\left\{\varsigma_k^{(n)}\right\}\right)}\right) + \frac{\frac{\rho_\text{u}\Omega(k)\left(\varsigma_k^{(n)}\right)^2}{H\left(\left\{\varsigma_k^{(n)}\right\}\right)}}{1 + \frac{\rho_\text{u}\Omega(k)\left(\varsigma_k^{(n)}\right)^2}{H\left(\left\{\varsigma_k^{(n)}\right\}\right)}}$$

$$\times \left(2 - \frac{\varsigma_k^{(n)}}{2\varsigma_k - \varsigma_k^{(n)}} - \frac{H(\{\varsigma_k\})}{H\left(\left\{\varsigma_k^{(n)}\right\}\right)}\right), \tag{25}$$

where $\left\{\varsigma_k^{(n)}\right\}$ is a feasible solution determined from the n-th iteration of P_2^{ZF} and

$$H(\{\varsigma_k\}) = \rho_\text{u} \sum_{i=1}^{K} \varsigma_i^2 c_i + 1. \tag{26}$$

Therefore, (22b) can be replaced with

$$\frac{1}{\ln 2}\mathcal{L}\left(\{\varsigma_k\}, \left\{\varsigma_k^{(n)}\right\}\right) \geq t_k, \ \forall k. \tag{27}$$

Since the QoS constraint in P_2^{ZF} can be represented as a second-order cone (SOC) [18], it is equivalent to

$$\sqrt{\rho_\text{u}\Omega(k)}\varsigma_k \geq \sqrt{\left(2^{\bar{R}_k} - 1\right)H(\{\varsigma_k\})}. \tag{28}$$

Hence, the $(n+1)$-th iteration of the proposed SCA method can be represented as

$$P_{2,n+1}^{\text{ZF}} : \max_{\{\varsigma_k, t_k\}} \sum_{k=1}^{K} t_k \tag{29a}$$

$$s.t. \quad 2\varsigma_k > \varsigma_k^{(n)}, \forall k \tag{29b}$$

$$(22d), (27), (28) \tag{29c}$$

Note that (29b) is due to $2x > \bar{x}$ in (24).

The problem (29) involves $2K$ scalar real variables, $2K$ quadratic constraints and $2K$ linear constraints, the complexity of each iteration is $\mathcal{O}\left((2K)^{4.5} + (2K)^{3.5}\right)$.

As such, the procedure for determining the problem P_2^{ZF} is summarized in the following Algorithm 1, shown at the top of

---

Algorithm 1 SCA algorithm for solving P_2^{ZF}

Choose a feasible solution $\left\{\varsigma_k^{(0)}, t_k^{(0)}\right\}$, define the error

tolerance ε and the number of iterations $\mathcal{N}$.

while $n \leq \mathcal{N}$ or $\left|\sum_{k=1}^{K}\left(t_k^{(n+1)} - t_k^{(n)}\right)\right| < \varepsilon$

Solve $P_{2,n+1}^{\text{ZF}}$ to obtain the solution $\left\{\varsigma_k^{(n+1)}, t_k^{(n+1)}\right\}$.

Reset $n := n + 1$.

end while

---

the next page.

Next, we analyze the convergence of Algorithm 1. Suppose $\{\varsigma_k\}$ is feasible to (29). By using (25), $\{\varsigma_k\}$ still satisfies (22b), which implies that $\{\varsigma_k\}$ is feasible to (22). In addition, since $\left\{\varsigma_k^{(n+1)}\right\}$ is an optimal solution to (29), it is also feasible to (22). It should be noticed that the sign '=' in (25) will happen when $\varsigma_k = \varsigma_k^{(n+1)}$. Thus, an optimal solution of the $(n+1)$-th iteration is also a feasible solution to the $(n+2)$-th iteration. Hence, the sequence generated by Algorithm 1 is monotonically increasing. In summary, the objective of Algorithm 1 is guaranteed to converge.

Remark 3: For a given rate QoS constraint $\bar{R}_k$, the feasible set of (22) is convex, therefore, the initial points for Algorithm 1 can be determined by solving a feasible SOCP. Besides, if the problem is infeasible, we simply let the total rate equal to 0.

C. One User's Rate Maximization for ZF Receiver

Without loss of generality, we assume the first user is the target user whose rate will be first guaranteed. Subjecting to the per-user power constraint and the QoS constraint, the rate maximization problem for the first user has the following form of

$$P_3^{\text{ZF}} : \max_{\{\eta_k\}} \log_2\left(1 + \frac{\rho_{\text{u}}\Omega(1)\eta_1}{\rho_{\text{u}}\sum_{i=1}^{K}\eta_i c_i + 1}\right) \tag{30a}$$

$$s.t. \quad R_k^{\text{ZF}} \geq \bar{R}_k, \ \forall k \neq 1 \tag{30b}$$

$$0 \leq \eta_k \leq 1, \ \forall k, \tag{30c}$$

where R_k^{ZF} is defined in (16). Utilizing the monotonicity of $\log_2(1+x)$ and performing some basic linear transformations, P_3^{ZF} is equivalent to

$$P_4^{\text{ZF}} : \min_{\{\eta_k, t\}} t \tag{31a}$$

$$s.t. \quad t^{-1}\eta_1^{-1}\sum_{i=1}^{K}\eta_i c_i(\Omega(1))^{-1} + t^{-1}\eta_1^{-1}(\rho_u\Omega(1))^{-1} \leq 1, \tag{31b}$$

$$\left(2^{\bar{R}_k} - 1\right)\left(\eta_k^{-1}\sum_{i=1}^{K}\eta_i c_i(\Omega(k))^{-1} + \eta_k^{-1}(\rho_u\Omega(k))^{-1}\right) \leq 1, \forall k \neq 1 \tag{31c}$$

$$0 \leq \eta_k \leq 1, \ \forall k. \tag{31d}$$

Obviously, P_4^{ZF} is a combination of monomials and polynomials, therefore, P_4^{ZF} is a standard GP. The solution of P_4^{ZF} can be

easily determined by using the CVX GP tool [19]. The algorithm for solving problem P_4^{ZF} is denoted by Algorithm 2.

IV. CB RECEIVER

In this section, it recalls a pre-studied uplink achievable closed-form rate expression for the CB receiver. This closed-form result enables us to design two optimal power optimization algorithms.

A. Achievable Rate for CB Receiver

The CB receiver for decoding the data signals is $\mathbf{A} = \hat{\mathbf{G}}$. With this receiver, r_k can be recast as

$$r_k^{\text{CB}} = \sqrt{\rho_{\text{u}}\eta_k}\hat{\mathbf{g}}_k^H\mathbf{g}_k q_k + \sqrt{\rho_{\text{u}}}\sum_{k'\neq k}^{K}\sqrt{\eta_{k'}}\hat{\mathbf{g}}_k^H\mathbf{g}_{k'}q_{k'} + \hat{\mathbf{g}}_k^H\mathbf{w}_{\text{u}}. \tag{32}$$

It is easy to find that the CB receiver cannot eliminate the inter-user interference. By treating the effective channel as the true channel and applying the worst Gaussian noise principle [13], Lemma 1 presents the achievable uplink per-user rate expression for the CB receiver.

Lemma 1: [20, Theorem 1] With CB receiver, a tight approximate uplink rate expression of the k-th user for any M, K, and N is formulated as

$$R_k^{\text{CB}} = \log_2\left(1 + \frac{\eta_k\|\boldsymbol{\ell}_{kk}\|_2^2}{\sum_{i\neq k}^{K}\eta_i\|\boldsymbol{\ell}_{ik}\|_2^2 + \frac{1}{N}\sum_{i=1}^{K}\eta_i\|\boldsymbol{\vartheta}_{ik}\|_2^2 + \frac{1}{N\rho_{\text{u}}}\|\boldsymbol{\ell}_{kk}\|_1}\right), \tag{33}$$

where

$$\boldsymbol{\ell}_{ik} = \left|\boldsymbol{\phi}_k^H\boldsymbol{\phi}_i\right|\left[\alpha_{1k}\frac{\beta_{1i}}{\beta_{1k}}, \alpha_{2k}\frac{\beta_{2i}}{\beta_{2k}}, ..., \alpha_{Mk}\frac{\beta_{Mi}}{\beta_{Mk}}\right]^T, \tag{34}$$

$$\boldsymbol{\vartheta}_{ik} = \left[\sqrt{\beta_{1i}\alpha_{1k}}, \sqrt{\beta_{2i}\alpha_{2k}}, ..., \sqrt{\beta_{Mi}\alpha_{Mk}}\right]^T. \tag{35}$$

Proof: See [20, Appendix A]. □

B. Total Rate Maximization for CB Receiver

Similar to P_1^{ZF}, the total rate maximization problem for the CB receiver has the following form of

$$P_1^{\text{CB}} : \max_{\{\eta_k\}} \sum_{k=1}^{K} R_k^{\text{CB}} \tag{36a}$$

$$s.t. \quad R_k^{\text{CB}} \geq \bar{R}_k, \ \forall k \tag{36b}$$

$$0 \leq \eta_k \leq 1, \ \forall k. \tag{36c}$$

Since P_1^{CB} is also non-convex with respect to η_k, we still adopt the SCA method to find a sub-optimum solution of P_1^{CB}. Defin-

ing $\zeta_k = \eta_k^{1/2}$, P_1^{CB} can be rewritten as

$$P_2^{\mathrm{CB}} : \max_{\{\zeta_k, t_k\}} \sum_{k=1}^{K} t_k \tag{37a}$$

$$s.t. \quad R_k^{\mathrm{CB}} \geq t_k, \ \forall k \tag{37b}$$

$$R_k^{\mathrm{CB}} \geq \bar{R}_k, \ \forall k \tag{37c}$$

$$0 \leq \zeta_k \leq 1, \ \forall k, \tag{37d}$$

where

$$R_k^{\mathrm{CB}} = \log_2 \left(1 + \frac{\zeta_k^2 \|\ell_{kk}\|_2^2}{\sum\limits_{i \neq k}^{K} \zeta_i^2 \|\ell_{ik}\|_2^2 + \frac{1}{N} \sum\limits_{i=1}^{K} \zeta_i^2 \|\vartheta_{ik}\|_2^2 + \frac{1}{N\rho_u} \|\ell_{kk}\|_1} \right). \tag{38}$$

By virtue of (24) and let $\left\{ \zeta_k^{(n)} \right\}$ be a feasible solution determined from the n-th iteration of P_2^{CB}, constraint (37b) can be recast as

$$\frac{1}{\ln 2} \mathcal{F} \left(\{\zeta_k\}, \left\{ \zeta_k^{(n)} \right\} \right) \geq t_k, \ \forall k, \tag{39}$$

where

$$\mathcal{F} \{\zeta_k\}, \left\{ \zeta_k^{(n)} \right\} \tag{40}$$

$$= \ln \left(1 + \frac{\left(\zeta_k^{(n)} \right)^2 \|\boldsymbol{\ell}_{kk}\|_2^2}{\mathcal{H} \left(\left\{ \zeta_k^{(n)} \right\} \right)} \right)$$

$$+ \frac{\frac{\left(\zeta_k^{(n)} \right)^2 \|\boldsymbol{\ell}_{kk}\|_2^2}{\mathcal{H} \left(\left\{ \zeta_k^{(n)} \right\} \right)}}{1 + \frac{\left(\zeta_k^{(n)} \right)^2 \|\boldsymbol{\ell}_{kk}\|_2^2}{\mathcal{H} \left(\left\{ \zeta_k^{(n)} \right\} \right)}} \left(2 - \frac{\zeta_k^{(n)}}{2\zeta_k - \zeta_k^{(n)}} - \frac{\mathcal{H} \left(\{\zeta_k\} \right)}{\mathcal{H} \left(\left\{ \zeta_k^{(n)} \right\} \right)} \right), \tag{41}$$

and

$$\mathcal{H} \left(\{\zeta_k\} \right) = \sum_{k' \neq k}^{K} \zeta_{k'}^2 \|\boldsymbol{\ell}_{k'k}\|_2^2 + \frac{1}{N} \sum_{k'=1}^{K} \zeta_{k'}^2 \|\boldsymbol{\vartheta}_{k'k}\|_2^2 + \frac{1}{\rho_u N} \|\boldsymbol{\ell}_{kk}\|_1. \tag{42}$$

Note constraint (37c) is also SOC representable [18], therefore, the $(n+1)$-th iteration of the SCA method for P_2^{CB} is expressed as

$$P_{2,n+1}^{\mathrm{CB}} : \max_{\{\zeta_k, t_k\}} \sum_{k=1}^{K} t_k \tag{43a}$$

$$s.t. \quad \zeta_k \|\boldsymbol{\ell}_{kk}\|_2 \geq \sqrt{\left(2^{\bar{R}_k} - 1 \right) \mathcal{H} \left(\{\zeta_k\} \right)}, \ \forall k \tag{43b}$$

$$2\zeta_k > \zeta_k^{(n)}, \forall k. \tag{43c}$$

$$(37\mathrm{d}), (39) \tag{43d}$$

The problem (42) involves $2K$ scalar real variables, $2K$ quadratic constraints, and $2K$ linear constraints, the complexity of each iteration is $\mathcal{O} \left((2K)^{4.5} + (2K)^{3.5} \right)$.

Algorithm 3 SCA algorithm for solving P_2^{CB}

Choose a feasible solution $\left\{ \varsigma_k^{(0)}, t_k^{(0)} \right\}$, define the error tolerance ε and the number of iterations $\mathcal{N}$.

while $n \leq \mathcal{N}$ or $\left| \sum\limits_{k=1}^{K} \left(t_k^{(n+1)} - t_k^{(n)} \right) \right| < \varepsilon$

Solve $P_{2,n+1}^{\mathrm{CB}}$ to obtain the solution $\left\{ \varsigma_k^{(n+1)}, t_k^{(n+1)} \right\}$.

Reset $n := n + 1$.

end while

As such, the algorithm for solving P_2^{CB} is obtained, shown at the top of this page.

Remark 4: The convergence analysis of Algorithm 3 is the same as that of Algorithm 1 and is omitted here due to space limitation. Besides, the initial points for starting Algorithm 3 can be also determined by solving a feasible SOCP.

C. One User's Rate Maximization for CB Receiver

Similar to P_3^{ZF}, the rate maximization problem for the first user with the CB receiver can be formulated as

$$P_3^{\mathrm{CB}} : \max_{\{\eta_k\}} R_1^{\mathrm{CB}} \tag{44a}$$

$$s.t. \quad R_k^{\mathrm{CB}} \geq \bar{R}_k, \ \forall k \neq 1 \tag{44b}$$

$$0 \leq \eta_k \leq 1, \ \forall k, \tag{44c}$$

where R_k^{CB} is given in (33). It observes that P_3^{CB} has the same structure as P_3^{ZF} and the standard GP form of P_3^{CB} is given by

$$P_4^{\mathrm{CB}} : \min_{\{\eta_k, t\}} t \tag{45a}$$

$$s.t. \quad \left(\sum_{i \neq 1}^{K} \boldsymbol{\eta}_i \|\boldsymbol{\ell}_{i1}\|_2^2 + \frac{1}{N} \sum_{i=1}^{K} \eta_i \|\boldsymbol{\vartheta}_{i1}\|_2^2 + \frac{1}{\rho_u N} \|\boldsymbol{\ell}_{11}\|_1 \right)$$
$$\times \|\boldsymbol{\ell}_{11}\|_2^{-2} t^{-1} \eta_1^{-1} \leq 1, \tag{45b}$$

$$\left(\sum_{i \neq 1}^{K} \eta_i \|\boldsymbol{\ell}_{ik}\|_2^2 + \frac{1}{N} \sum_{i=1}^{K} \eta_i \|\boldsymbol{\vartheta}_{ik}\|_2^2 + \frac{1}{\rho_u N} \|\boldsymbol{\ell}_{kk}\|_1 \right)$$
$$\times \|\boldsymbol{\ell}_{kk}\|_2^{-2} \left(2^{\bar{R}_k} - 1 \right) \eta_k^{-1} \leq 1, \ \forall k \neq 1 \tag{45c}$$

$$0 \leq \eta_k \leq 1, \ \forall k. \tag{45d}$$

The solution of P_4^{CB} can also be determined by using the CVX GP tool [19]. We denote the algorithm for solving P_4^{CB} by Algorithm 4.

V. SIMULATION RESULTS

In this section, a comprehensive uplink rate performance comparison between the ZF and CB receivers is performed. This comparison studies design issues surrounding the number of APs, the power control strategies, and the different receiver techniques.
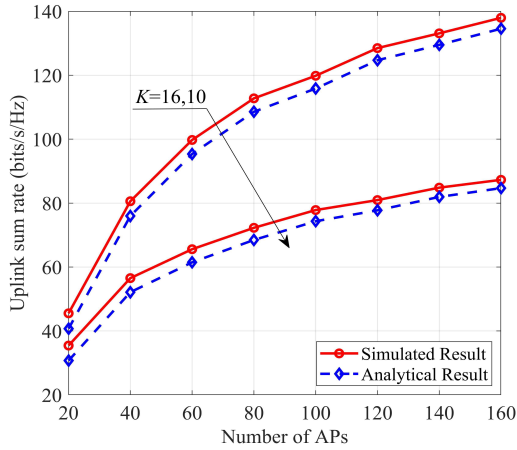
Fig. 1. The relationships between the sum rate and the number of APs for different K. Here all pilots are mutually orthogonal and $N = 2$.
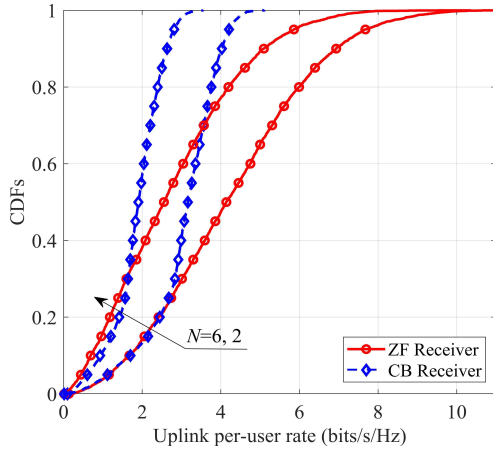

Fig. 3. CDFs of achievable uplink per-user rate for the ZF and CB receivers for different τ. Here $M = 60$, $K = 10$ and $N = 6$.

Fig. 2. CDFs of achievable uplink per-user rate for the ZF and CB receivers for different N. Here $M = 60$ and $K = 10$.

Fig. 4. The total power consumptions versus the number of APs for different N. Here $K = 10$.

A. Simulation Parameters

We consider a 1 km × 1 km square area for simulation, which is wrapped-around to imitate an infinite network environment. The large-scale fading coefficient is modeled by

$$\beta_{mk} = \mathrm{PL}_{mk} \cdot 10^{\frac{\sigma_{\mathrm{sh}} z_{mk}}{10}}, \tag{46}$$

where PL_{mk} is the path loss between the m-th AP and k-th user and $10^{\sigma_{\mathrm{sh}} z_{mk}/10}$ denotes the shadow fading with a standard deviation σ_{sh}. We adopt the three-slope path loss model given in [1]. For all examples without special explanation, Table 1 enumerates the system parameters appeared in this paper.

For the case of no power optimization, we adopt the equal power coefficient (EPC) scheme given in [1]. In this strategy, all power coefficients are set to 1, *i.e.*, $\eta_k = 1, \forall k$.

B. Performance Evaluation

In Fig. 1, the sum rate comparison between the "Simulated Result" in (14) and the "Analytical Result" in (16) for different M and K is presented. Here we assume all pilots are mutually orthogonal and $N = 2$. Note the "Simulated Result" is gener-
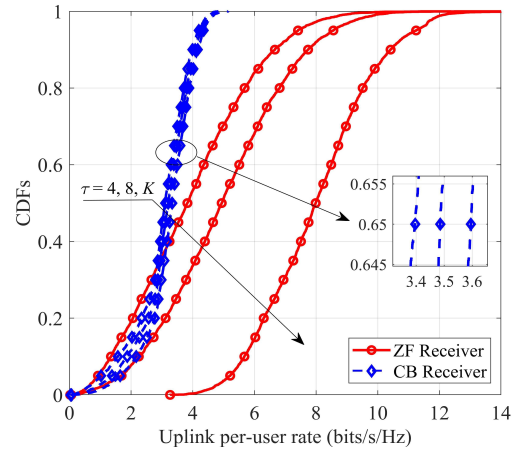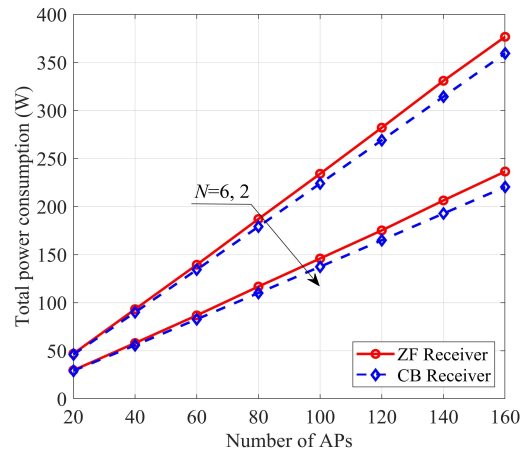
Table 1. System Parameters.

Parameter	Value
N_0 (noise power)	$290 \times \kappa \times B \times NF$
κ, B, NF	Boltzmann constant, 20 MHz, 9 dB
$\tau, \rho_{\mathrm{p}}, \rho_{\mathrm{u}}$	K / 2, 100, 100 mW
σ_{sh}	8 dB

ated by using the Monte-Carlo simulation technique by averaging 10^3 independent channel realizations. As we can see, the relative performance gap between (14) and (16) is marginal in all considered cases compared to the achievable sum rate, which indicates that our closed-form result in (16) is a good predictor to approximate the ergodic rate (14). In addition, we find the sum rate is an increasing function of M. This is because the larger M promises more antenna array gains, thereby bringing more degree-of-freedoms to resist the fading and interference.

Fig. 2 depicts the cumulative distribution functions (CDFs) of the achievable uplink per-user rate for different N under the EPC scheme, with $M = 60$ and $K = 10$. As expected, the ZF receiver outperforms the CB receiver except for the low-SINR regime. This is because in low SINR regime, although the ZF
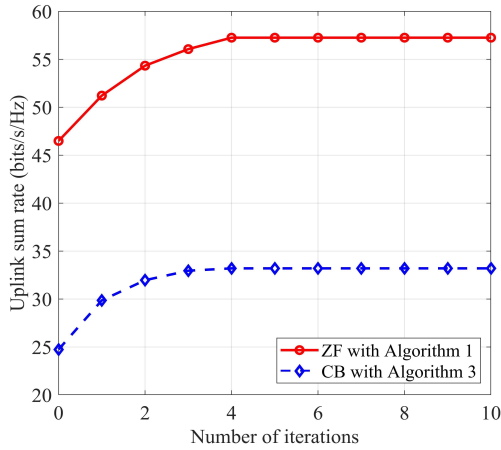
Fig. 5. The convergence of Algorithms 1 and 3. Here $M = 60$, $K = 10$, $N = 6$ and $\bar{R}_k = 1$ bits/s/Hz.

Fig. 6. Uplink sum rate versus the number of APs. Here $K = 10$, $N = 6$ and $\bar{R}_k = 1$ bits/s/Hz.

receiver cancels the inter-user interference, it inevitably amplifies the thermal noise. It is also interesting to notice that, when N increases from 2 to 6, the merits of the ZF receiver in the low-SINR regime also appears. This finding shows that using additional antennas at the APs can compensate for the performance loss due to the additive noise. When implementing the ZF receiver, more users can enjoy the high-SINR service. For instance, when $N = 6$, more than 52% of users have reached a rate of 4 bits/s/Hz for the ZF receiver. But for the CB receiver, this ratio is only 10%. These above insights demonstrate the superiority of the ZF receiver.

In Fig. 3, the CDFs of the achievable uplink per-user rate for the ZF and CB receivers against different channel estimation error under the EPC scheme are plotted, with $M = 60$, $K = 10$ and $N = 6$. Here we represent different channel estimations by changing the value of τ. Since the CPU randomly allocates pilots to the user, when $\tau < K$, the smaller the τ is, the more likely the same pilot is to be used by more users, resulting in more serious pilot contamination. Note when $\tau = K$, there is no pilot contamination. It is clear to see that the performance of the ZF receiver is dominated by the accuracy of the channel estimation. When we narrow the value of τ for the ZF receiver, the corresponding performance will drop dramatically. For instance, when τ is reduced from 10 to 8, the 5%-outage and median rates of the ZF curve have decreased 208.4% and 62.1%, respectively. This insightful observation reveals that the ZF receiver is sensitive to the channel detection errors. In addition, compared with the ZF receiver, the CB receiver is more robust on the channel estimation errors. Nevertheless, the CB receiver suffers from severe inter-user interference and hence, results in unsatisfactory rate performance.

Fig. 4 explores the total power consumptions of the ZF and CB receivers against the number of APs for different N under the EPC scheme, with $K = 10$. Here we adopt the generic power model given in [12, Section III]. As we can see, the total power cost of the ZF receiver is always higher than the CB receiver. While as the number of APs increases, the relative power gap between these two receivers increases. This is due to the fact that the ZF receiver requires extra power to suppress
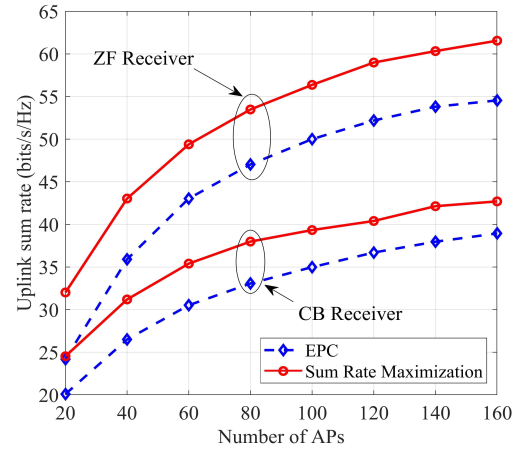
interference from other users. In fact, since the merits of the ZF receiver gradually appear with the increasing of the number of APs, it is advisable to use more power to promise a huge performance gain.

Until now, we have investigated the rate performance of the ZF and CB receivers without any power optimization. The ZF receiver benefits from the cancellation of the inter-user interference, promising huge performance enhancement in the high-SINR regime. Next, we first evaluate the effectiveness of the Algorithms 1 and 3 in maximizing the total rate for these two receivers as well as their convergence rates. Fig. 5 depicts numerically the total rate versus the number of iterations, with $M = 60$, $K = 10$, $N = 6$ and $\bar{R}_k = 1$ bits/s/Hz. It can be easily concluded that both Algorithms 1 and 3 only need a few iterations to converge. The total rate tends to a stable value after 4 iterations, which demonstrates that our proposed algorithms have a fast converge rate. We then compare our Algorithms 1 and 3 with the EPC scheme to further highlight the effectiveness of our algorithms. Fig. 6 shows the relative performance gaps between the EPC and Algorithms 1 and 3 against the number of APs, with $K = 10$, $N = 6$ and $\bar{R}_k = 1$ bits/s/Hz. It can be observed that, compared with the EPC scheme, Algorithms 1 and 3 have the ability to significantly improve the total rate and the rate improvement of the ZF receiver is better than the CB receiver. In addition, it is also interesting to notice for all considered cases, the relative performance gap between these two receivers increases as the number of APs increases. This is because as the number of APs increases, the channel hardening becomes more pronounced, thereby reducing the channel estimation errors. Benefiting from smaller channel estimation errors, the total antenna array has a stronger ability to resist the inter-user interference, resulting in significant performance gains in terms of the sum rate. The same insight can also be obtained by using more antennas at each AP, see Fig. 2.

To conclude this paper, we examine the effectiveness of Algorithms 2 and 4. Table 2 presents the achievable uplink per-user rate of the proposed Algorithms 2 and 4, with $M = 60$, $K = 10$, $N = 6$ and $\bar{R}_k = 1$ bits/s/Hz. Note different channel realizations in Table 2 correspond to different APs'

Table 2. Achievable uplink per-user rate for Algorithms 2 and 4. Here $M = 60$, $K = 10$, $N = 6$ and $\bar{R}_k = 1$ bits/s/Hz.

| Receiver | Channel | Achievable uplink per-user rate (bits/s/Hz) | | | | | | | | | |
		User 1	User 2	User 3	User 4	User 5	User 6	User 7	User 8	User 9	User 10
	1	9.881	1.000	1.000	1.000	1.000	1.000	1.000	1.000	1.000	1.000
ZF	2	9.505	1.000	1.000	1.000	1.000	1.000	1.000	1.000	1.000	1.000
	3	7.859	1.000	1.000	1.000	1.000	1.000	1.000	1.000	1.000	1.000
	1	3.277	1.000	1.000	1.000	1.000	1.000	1.000	1.000	1.000	1.000
CB	2	4.032	1.000	1.000	1.000	1.000	1.000	1.000	1.000	1.000	1.000
	3	2.936	1.000	1.000	1.000	1.000	1.000	1.000	1.000	1.000	1.000

and users' locations (which are randomly generated in this simulation), thus leading to different large-scale fading coefficients. As expected, in all considered cases, the rate of user 1 has maximized after using the proposed algorithms while the rate of the remaining users can satisfy their QoS constraints. In addition, Table 2 also implies that the ZF receiver is always superior to the CB receiver in the high-SINR regime, which coincides with the conclusion drawn from Figs. 2 and 3.

VI. CONCLUSIONS

In this paper, we investigated the uplink rate performance of cell-free mMIMO system with the ZF and CB receivers. A novel tight approximate rate expression for the ZF receiver was derived. Compared with the CB receiver, the ZF receiver benefited from eliminating the inter-user interference, thereby improving the system performance. In addition, by leveraging on the derived rate expressions, two power control algorithms were proposed, subjecting to the user power constraints and the QoS constraints. We found the total rate maximization algorithms have a fast convergence rate. Moreover, the proposed sum rate maximization algorithms can significantly enhance the sum rate for both ZF and CB receivers compared to the EPC scheme. Furthermore, we also observed the one user's rate maximization algorithms work well in many respects.

APPENDIX A
Proof of Theorem 1

Firstly, by defining

$$c_i = \arg\max_m \left(\beta_{mi} - \alpha_{mi} \right), \tag{47}$$

we obtain

$$R_k^{\mathrm{ZF}} \geq \mathbb{E} \left\{ \log_2 \left(1 + \frac{\rho_{\mathrm{u}} \eta_k}{\left(\rho_{\mathrm{u}} \sum_{i=1}^{K} \eta_i c_i + 1 \right) \|\mathbf{a}_k\|^2} \right) \right\}. \tag{48}$$

Since $-\log_2 (1 + 1/x)$ is a convex function with respect to x and by virtue of the Jensen's Inequality, we have

$$R_k^{\mathrm{ZF}} \geq \log_2 \left(1 + \frac{\rho_{\mathrm{u}} \eta_k}{\left(\rho_{\mathrm{u}} \sum_{i=1}^{K} \eta_i c_i + 1 \right) \mathbb{E} \left\{ \|\mathbf{a}_k\|^2 \right\}} \right). \tag{49}$$

From (4) and (5), it remarks that the channel estimations of two users using the same pilot sequence are parallel. In other words,

if $\phi_k = \phi_j, \forall k \neq j$, it yields

$$\hat{\mathbf{g}}_{mk} = \frac{\beta_{mk}}{\beta_{mj}} \hat{\mathbf{g}}_{mj}. \tag{50}$$

Expression (50) indicates that $\hat{\mathbf{G}}$ is rank-deficient, therefore the property of Wishart matrix can not be utilized.

Next, leveraging on [21, Eq. (62)], $1/\|\mathbf{a}_k\|^2$ can be approximated by

$$\frac{1}{\|\mathbf{a}_k\|^2} \approx \|\hat{\mathbf{g}}_k\|^2 - \sum_{j \neq k}^{K} \hat{\mathbf{g}}_k^H \hat{\mathbf{g}}_j \frac{1}{\|\hat{\mathbf{g}}_j\|^2} \hat{\mathbf{g}}_j^H \hat{\mathbf{g}}_k$$

$$= \|\hat{\mathbf{g}}_k\|^2 - \sum_{j \neq k}^{K} \sum_{n=1}^{N} \left| \left[\hat{\mathbf{g}}_{m_{j*}k} \right]_n \right|^2$$

$$= \sum_{m \in \mathcal{M}_k} \sum_{n=1}^{N} \left| \left[\hat{\mathbf{g}}_{mk} \right]_n \right|^2, \tag{51}$$

where

$$m_{j*} = \arg\max_m \beta_{mj}, \tag{52}$$

$$\mathcal{M}_k = \left\{ \forall m \neq m_{j*} | j \neq k \right\}. \tag{53}$$

Since the norm of circularly symmetric complex Gaussian variable obeys Gamma distortion, it yields

$$\left| [\hat{\mathbf{g}}_{mk}]_n \right| \sim \Gamma \left(1, \alpha_{mk} \right). \tag{54}$$

The above expression allows us to obtain an approximate distribution of $1/\|\mathbf{a}_k\|^2$, as

$$\frac{1}{\|\mathbf{a}_k\|^2} \sim \Gamma \left(\frac{N \left(\sum_{m \in \mathcal{M}_k} \alpha_{mk} \right)^2}{\sum_{m \in \mathcal{M}_k} \alpha_{mk}^2}, \frac{\sum_{m \in \mathcal{M}_k} \alpha_{mk}^2}{\sum_{m \in \mathcal{M}_k} \alpha_{mk}} \right). \tag{55}$$

By virtue of the property of the Gamma function, we obtain

$$\frac{1}{\mathbb{E} \left\{ \|\mathbf{a}_k\|^2 \right\}} = \frac{\sum_{m \in \mathcal{M}_k} \alpha_{mk}^2}{\sum_{m \in \mathcal{M}_k} \alpha_{mk}} \left(\frac{N \left(\sum_{m \in \mathcal{M}_k} \alpha_{mk} \right)^2}{\sum_{m \in \mathcal{M}_k} \alpha_{mk}^2} - 1 \right). \tag{56}$$

Plugging (56) into (49), (16) is obtained.

REFERENCES

[1] H. Q. Ngo, A. Ashikhmin, H. Yang, E. G. Larsson, and T. L. Marzetta, "Cell-free massive mimo versus small cells," *IEEE Trans. Wireless Commun.,* vol. 16, no. 3, pp. 1834–1850, Mar. 2017.

[2] H. Yang and T. L. Marzetta, "Energy efficiency of massive mimo: Cell-free vs. cellular," in *Proc. IEEE VTC,* June 2018, pp. 15–64.

[3] H. Q. Ngo, L. Tran, T. Q. Duong, M. Matthaiou, and E. G. Larsson, "On the total energy efficiency of cell-free massive mimo," *IEEE Trans. Green Commun. Netw.,* vol. 2, no. 1, pp. 25–39, Mar. 2018.

[4] E. Nayebi, A. Ashikhmin, T. L. Marzetta, H. Yang, and B. D. Rao, "Precoding and power optimization in cell-free massive mimo systems," *IEEE Trans. Wireless Commun.,* vol. 16, no. 7, pp. 4445–4459, July 2017.

[5] Y. Li and G. A. A. Baduge, "NOMA-aided cell-free massive MIMO systems," *IEEE Wireless Commun. Lett.,* vol. 7, no. 6, pp. 950–953, Dec. 2018.

[6] Q. Huang and A. Burr, "Compute-and-forward in cell-free massive MIMO: Great performance with low backhaul load," in *Proc. IEEE ICC Workshops,* May 2017, pp. 601–606.

[7] M. Bashar, K. Cumanan, A. G. Burr, H. Q. Ngo, and M. Debbah, "Cell-free massive MIMO with limited backhaul," in *Proc. IEEE ICC,* May 2018, pp. 1–7 .

[8] P. Liu, K. Luo, D. Chen, and T. Jiang, (May 2018), "Spectral efficiency analysis in cell-free massive MIMO systems with zero-forcing detector", [online] Available: https://arxiv.org/abs/1805.10621.

[9] J. Zhang, Y. Wei, E. Björnson, Y. Han, and X. Li, "Spectral and energy efficiency of cell-free massive MIMO systems with hardware impairments," in *Proc. IEEE WCSP,* Oct. 2017, pp. 1–6.

[10] M. Bashar, K. Cumanan, A. G. Burr, M. Debbah, and H. Q. Ngo, "Enhanced max-min SINR for uplink cell-free massive MIMO systems," in *Proc. IEEE ICC,* May 2018, pp. 1–6.

[11] T. H. Nguyen, T. K. Nguyen, H. D. Han, and V. D. Nguyen, "Optimal power control and load balancing for uplink cell-free multi-user massive MIMO," *IEEE Access,* vol. 6, pp. 14462–14473, Feb. 2018.

[12] Y. Zhang, H. Cao, M. Zhou, and L. Yang, "Power optimization for energy efficiency in cell-free massive MIMO with ZF receiver," in *Proc. IEEE ICACT*, Feb. 2019, pp. 366–371.

[13] T. L. Marzetta, E. G. Larsson, H. Yang, and H. Q. Ngo, *Fundamentals of Massive MIMO.* Cambridge, U.K.: Cambridge Univ. Press, 2016.

[14] Z. Luo and S. Zhang, "Dynamic spectrum management: Complexity and duality", *IEEE J. Sel. Topics Signal Process.,* vol. 2, no. 1, pp. 57–73, Feb. 2008.

[15] A. Beck, A. Ben-Tal, and L. Tetruashvili, "A sequential parametric convex approximation method with applications to nonconvex truss topology design problems," *J. Glob. Optim.,* vol. 47, no. 1, pp. 29–51, May 2010.

[16] G. Scutari, F. Facchinei, and L. Lampariello, "Parallel and distributed methods for constrained nonconvex optimization–Part I: Theory," *IEEE Trans. Signal Process.,* vol. 65, no. 8, pp. 1929–1944, Apr. 2016.

[17] H. Tuy, *Convex Analysis and Global Optimization.* MA, Boston: Kluwer, 1998.

[18] S. Boyd and L. Vandenberghe, *Convex Optimization.* Cambridge, U.K.: Cambridge Univ. Press, 2004.

[19] M. Grant and S. Boyd, CVX: Matlab software for disciplined convex programming, version 2.0 beta, Sept. 2013. Available: http://cvxr.com/cvx.

[20] M. Bashar, K. Cumanan, A. G. Burr, H. Q. Ngo, and H. V. Poor, "Mixed quality of service in cell-free massive MIMO," *IEEE Commun. Lett.,* vol. 22, no. 7, pp. 1494–1497, July 2018.

[21] J. Wang and L. Dai, "Asymptotic rate analysis of downlink multi-user systems with co-located and distributed antennas," *IEEE Trans. Wireless Commun.,* vol. 14, no. 6, pp. 3046–3058, June 2015.

Yao Zhang received the B.S. degree in College of Computer Science & Technology from Qingdao University, China, in 2016. He is currently pursuing his Ph.D. degree at the Department of Communication and Information Engineering in Nanjing University of Posts and Telecommunications. His research interests include massive MIMO, especially power optimization in cell-free massive MIMO.

Haotong Cao received B.S. degree in Communication Engineering from Nanjing University of Posts and Telecommunications (NJUPT) in 2015. He is currently pursuing his Ph.D. Degree in NJUPT, Nanjing, China. He was a Visiting Scholar of Loughborough University, U.K. in 2017. He has served as the TPC member of multiple IEEE conferences, such as IEEE INFOCOM, IEEE ICC, IEEE Globecom. He is also serving as the reviewer of multiple academic journals, such as IEEE/ACM Transactions on Networking, IEEE Transactions on Network and Service Management and (Elsevier) Computer Networks. He has published multiple IEEE Trans./Journal/Magazine papers since 2016. His research interests include wireless communication theory, resource allocation in wired and wireless networks. He has been awarded the 2018 Postgraduate National Scholarship of China. He has been awarded 2019 IEEE ICC SecSDN Workshop Best Paper Award.

Meng Zhou received the M.S. degree from Northwest Normal University, Lanzhou, China, in 2018. He is presently pursuing the Ph.D. degree with the College of Communication and Information Engineering from the Nanjing University of Posts and Telecommunications (NJUPT), Nanjing, China. His broad interests in wireless communications, with a special interest of cell-free massive MIMO, resource allocation, physical layer security, HetNets in B5G and 6G.

Longxiang Yang is currently with the College of Telecommunications and Information Engineering, Nanjing University of Posts and Telecommunications (NJUPT), Nanjing, China. He is a Full Professor and Doctoral Supervisor of NJUPT. He is also the Vice-President of College of Telecommunications and Information Engineering, NJUPT. He has fulfilled multiple National Natural Science Foundation projects of China. He has authored and co-authored over 200 technical papers published in various journals and conferences. His research interests include cooperative communication, network coding, wireless communication theory, B5G and 6G mobile communication systems, ubiquitous networks and Internet of things.